CrossMark

ORIGINAL PAPER

Isolating the location of scour-induced stiffness loss in bridges using local modal behaviour

Luke J. Prendergast[1] · Kenneth Gavin[1] · David Hester[2]

Abstract Detecting scour by analysing bridge vibrations is receiving an increasing amount of attention in the literature. Others have considered changes in natural frequency to indicate the presence of scour damage; however, little work has been reported on identifying the location of a scour hole based on vibration measurements. In this paper, a numerical study is carried out using a bespoke vehicle–bridge–soil dynamic interaction model to examine how the first six vibration modes (Eigen frequencies) of a typical integral bridge are affected by scour at different locations. It is found that depending on the location of the scour hole, some modes are much more affected than others in terms of frequency changes. In fact, a clear pattern emerges as to which modes are affected by which scour location. Using this knowledge, the location of a scour hole can potentially be detected on a real bridge. However, recognising that it is not possible to undertake an eigenvalue analysis on an actual bridge, an analysis is performed by collecting acceleration signals from various points on the structure. The bridge is loaded by a realistic vehicle model, incorporating vehicle–bridge interaction effects, which leads to

the generation of discrete acceleration signals at various 'sensor' locations on the bridge. In this paper, it is found that it is possible to detect the location of a scour hole using a relatively small number of 'sensors'. However, to achieve this, careful signal processing is necessary and advice on a number of pertinent issues is provided.

1 Introduction

1.1 Bridge scour

Scour erosion of bridge foundation soil is the number one cause of bridge failure in bridges located over waterways [1–3]. One study found that 53% of 500 bridge failures occurring between 1989 and 2000 in the United States occurred as a result of flooding and/or scour problems [4]. This issue presents a significant cost burden on bridge owners/managers worldwide between inspections, scour protection installation and repairing damage caused by scour [5]. Scour failures typically occur quite suddenly and generally without prior warning, which can potentially lead to loss of life. The potentially serious consequences of scour have resulted in significant research efforts in the area and an overview of this work is given herein. Previous work can broadly be classified into two groups: (1) methods which directly measure scour depth using instrumentation, and (2) indirect methods which infer scour severity by tracking changes in bridge modal properties, e.g. natural frequency. To give context to the current work, Sects. 1.2 and 1.3 provide an overview of previous work on direct measurement approaches [category (1)], and indirect

✉ Luke J. Prendergast
  l.j.prendergast@tudelft.nl

  Kenneth Gavin
  k.g.gavin@tudelft.nl

  David Hester
  d.hester@qub.ac.uk

[1] Faculty of Civil Engineering and Geosciences, Delft University of Technology, Building 23, Stevinweg 1, PO-box 5048, 2628 CN Delft, The Netherlands

[2] School of Natural and Built Environment, Queen's University Belfast, University Road, Belfast BT7 1NN, Northern Ireland, UK

measurement approaches [category (2)], respectively. Finally, Sect. 1.4 gives an overview of the present article.

1.2 Direct monitoring of bridge scour using depth-measuring instrumentation

A range of sensors and methods have been developed to monitor scour hole progression [5]. Simple systems such as Float-Out Devices and Tethered Buried Switches [6, 7] float out of the soil when scour reaches their installed depth, triggering a signal. Time-Domain Reflectometry (TDR) systems use changes in dielectric permittivity to monitor the location of the soil–water interface relative to a fixed probe [8, 9]. Similarly, Ground Penetrating Radar (GPR) can be used to detect scour holes using high frequency electromagnetic waves, which are partially reflected as they pass through different media [3, 10]. Sound wave devices such as Sonic Fathometers [5, 9, 11], Reflection Seismic Profilers [5, 10] and Echo Sounders [10] emit sonic pulses to locate the soil–water interface and, hence, the scour depth, using a similar approach to the radar methods. A variety of methods rely on the installation of rods into the soil near a foundation. Magnetic Sliding Collars (MSC) [5, 7] involve monitoring the movement of a gravity-controlled sensor which sits on the streambed surrounding a rod. The sensor falls with increasing scour depth relative to the rod and closes magnetic switches along the rod, indicating its depth. The Wallingford 'Tell-Tail' Device [12] consists of motion sensors tethered to a rod that detect bed movements as sediments are scoured to their level. Zarafshan et al. [13] developed a system which uses changes in the vibration frequency of a driven rod to detect scour, as measured using a Fibre-Bragg Grating (FBG) sensor. The method allows for the scour depth to be identified via the creation of a Winkler-based model of the soil-rod system. The Winkler coefficient of subgrade reaction is calibrated from the frequency measured at installation of the system, allowing direct monitoring of scour depth based on the changes in frequency measured.

1.3 Indirect monitoring of bridge scour by identifying changes in bridge modal properties

Several authors have investigated the effects of scour on bridge structural performance characteristics both numerically and experimentally. The lateral response of bridges subjected to extreme scour was investigated numerically by Klinga and Alipour [14], who focussed on the performance of a number of bridge elements (abutments, piles and the superstructure) under extreme scour. The study concluded that as scour depth increases the lateral stiffness of the bridge decreases as does its natural frequency. Ju [15]

conducted a study of the changes in natural frequency of a bridge due to scour incorporating soil–fluid–structure interaction, and concluded that the presence of water around foundation elements leads to lower natural frequency values than the absence of water due to water-added mass effects. However, accounting for this effect is not trivial and can be neglected in bridge natural frequency analysis. Prendergast et al. [16] describe a numerical study into monitoring scour around the central pier of a two-span integral bridge using vehicle-induced vibrations. The work focusses on detecting changes in the first natural frequency of the bridge using a single 'sensor' (virtual node point in numerical model) located on the pier and also investigates the influence of foundation soil stiffness on the method.

Other authors have investigated the effect of scour using experimental testing to complement numerical analysis. Chen et al. [17] describe a vibration-based scour evaluation method applied to a cable-stayed bridge using ambient velocity measurements. Combining sensor measurements with finite-element updating, the scour condition of one of the piers was successfully detected. Briaud et al. [6] investigated the use of scour monitoring instrumentation on a laboratory scale bridge constructed in a large hydraulic flume. Both shallow and deep foundation types were investigated. The study concluded that accelerometers located on the model bridge pier performed very well at measuring the change in natural frequency as scour severity increased. Using full-scale field testing Prendergast et al. [18] validated a method to detect the change in the natural frequency of a single pile affected by scour. Moreover, they suggest a method for creating soil-springs using correlations to geotechnical site data such as shear-wave velocities and cone penetration tests. Foti and Sabia [19] describe an investigation carried out on a five-span bridge adversely affected by scour during a major flood. Prior to a planned retrofit, one of the pier responses was monitored to ascertain if scour could be detected by utilising the asymmetric (rigid-body) dynamic behaviour of the pier and analysing foundation acceleration signals. The study concluded that the presence of scour was detectable but its extent was not. Elsaid and Seracino [20] conducted a study of the scour effect on the dynamic response of a scaled-model of a steel bridge, and concluded that horizontally displaced mode shapes showed sensitivity to scour progression, with vertical modes being predominately unaffected. This study did not consider any soil–structure interaction, however, and instead they simulated scour as the increase in effective length of the piles.

1.4 Overview of current study

The work of authors [6, 14–20] shows that there is a general agreement that changes in natural frequency offer

potential as a method to remotely detect and monitor the presence of scour around a foundation element. However, to date no research has been undertaken into using changes in natural frequency as a method to *locate* a scour hole (i.e. determining whether the scour occurs around a certain abutment or pier) and, therefore, that is the primary focus of this paper. This is important since knowledge of the location of a scour hole is as significant to bridge managers as monitoring the evolution of known scour. In this paper, a novel method to locate a scour hole using a small number of 'sensors' is proposed. The word sensor refers, in the context of this paper, to a virtual node point in a numerical model. Studies are undertaken to identify the *location* of a scour hole around a typical two-span integral bridge by analysing signals from the structure due to a passing realistic vehicle model. Vehicle–bridge interaction effects are incorporated to make the model outputs as realistic as possible. An integral bridge is purposefully chosen as (1) the horizontal response may be more readily excited by a passing vehicle due to the moment connections between the substructure and the deck, (2) various modes of an integral bridge are affected independently by scour at different locations and utilising knowledge of these modal changes can isolate scour hole location and (3) integral bridges are becoming much more commonly constructed due to the ease of maintenance and lack of expansion joints. The analysis builds on work presented in Prendergast et al. [16], which proposed a method to identify the occurrence of scour at some part of the substructure using a single sensor, and expands the approach to locating scour using distributed sensors. Challenges related to bridge spectra being contaminated by vehicle-induced frequencies, where to locate 'sensors' and required time-length of signals, are also investigated in this paper. Though an overarching methodology is not proposed, guidance on several issues is provided. The modelling methods employed are presented in the next section.

2 Finite-element modelling

A numerical model of a bridge incorporating small-strain foundation soil stiffness and a realistic vehicle load model is developed using MATLAB. The structure modelled is a two-span integral bridge founded on piles. The vehicle is modelled as a sprung 2 axle system and the effects of vehicle–bridge interaction are incorporated, resulting in a significantly more realistic simulation of the loading than using constant axle loads. The various model components and their formulation in the numerical environment are discussed in the following sub-sections, namely bridge structural modelling, soil–structure interaction, and vehicle–bridge interaction.

2.1 Bridge structural modelling

The bridge modelled is a two-span integral bridge, see Fig. 1. A full description of the model development is available in [21]; however, for completeness some details are provided herein. The bridge deck is modelled using nine U10 concrete bridge beams, see [22]. The bridge beams support a 200 mm deep concrete deck slab. The bridge contains two abutments; each one is composed of a series of nine vertical concrete columns supporting the individual deck beams. Each column is cast in a sleeve and surrounded by reinforced earth. The concrete sleeve permits lateral movement of the columns to accommodate thermal expansion, as a traditional expansion joint is not included on bridges of this type. Since on a real bridge the stiffness of each abutment will not be exactly equal (due to minor differences in the soil conditions, material properties, etc.), the flexural rigidity of each abutment is varied by ±10%. The stiffness of the LHS abutment is reduced by 10%, whereas the stiffness of the RHS abutment is increased by 10%. The bridge deck is supported in the centre by two stiff piers, which provide longitudinal restraint to the bridge deck. The abutment columns rest on a strip pilecap, which is supported by ten 15 m long concrete piles (two rows × five piles). The central pier system comprises two separate leaves, each resting on an individual pilecap. Each leaf is supported by four 15 m long piles, arranged in a square formation. The main properties adopted in the numerical model are outlined in Table 1.

For the purpose of modelling, the structure is idealised as a 2-D frame. Admittedly a 2-D model cannot capture all the nuances of the 3-D bridge behaviour. However, for the purpose of this study the 2-D model is able to capture the phenomena being studied as the responses of interest take place in the longitudinal (traffic) direction while "into the page" and torsional behaviour is not targeted. Moreover, using a 2-D model allows for high-speed computation of the dynamic responses and the model properties (span lengths, number of spans, pile lengths, etc.) can be tailored quickly and efficiently if needed. To effectively reduce the structure to 2-D, grouped geometric properties (moment of inertia, cross-sectional area etc.) are used to model the structural behaviour of the deck, pier, abutments and piles. For example, the nine abutment columns in Fig. 1 can be modelled as a single line of elements in Fig. 2 by summing the individual areas and moments of inertia, respectively. Modelling the structure as a 2-D frame has the drawback that the scour effect introduced is assumed to occur along the entire length of a given support. The pile groups are assumed to act as block elements, whereby the properties of the group (stiffness, mass, etc.) are attributed to a line of elements for each set of piles (see Fig. 2). The structural elements are modelled using 6-degree-of-freedom (6-DOF)
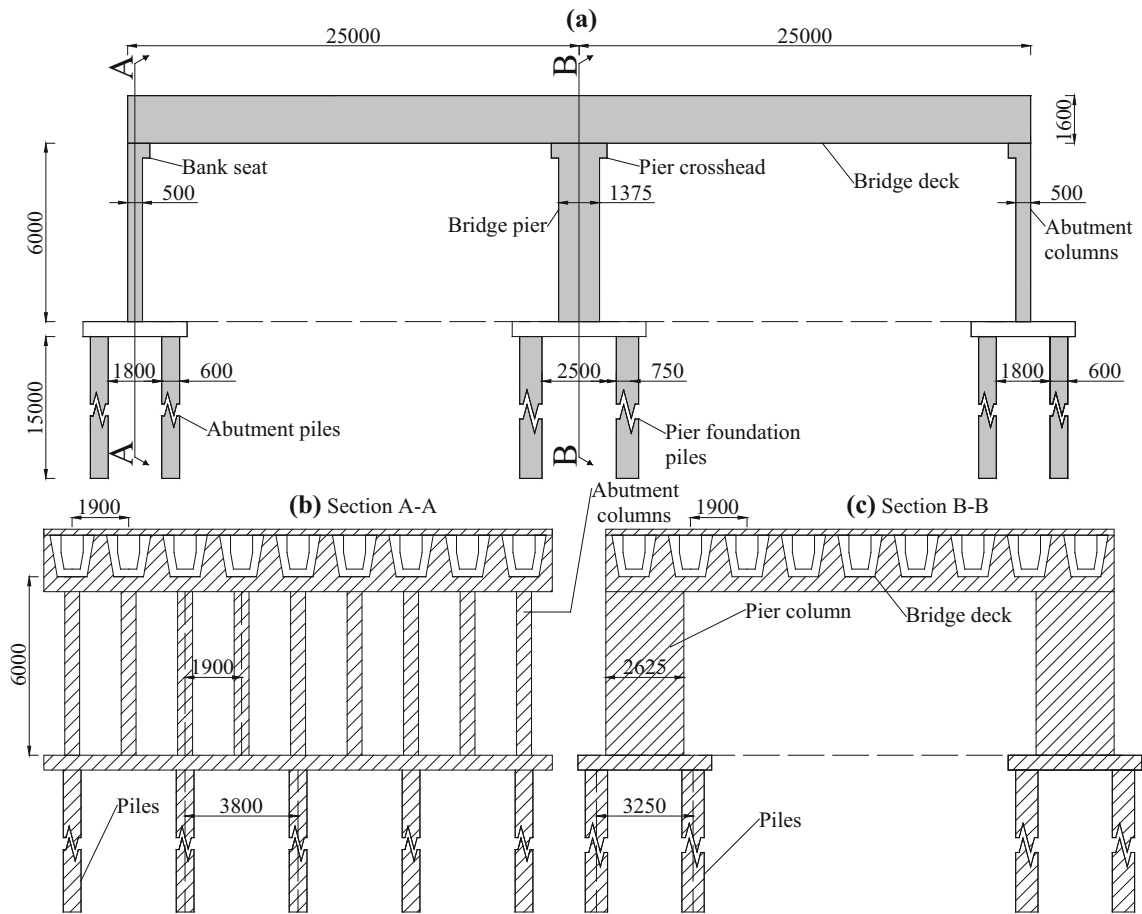
Fig. 1 Bridge model used in numerical simulations. **a** Bridge elevation, **b** section A–A, **c** section B–B

Table 1 Bridge properties

Element	Property	Value
Bridge deck elements	EI (kN m^2)	1.032×10^8
	ρA (kg m)	2.284×10^4
LHS abutment elements	EI (kN m^2)	869,400
	ρA (kg m)	4.241×10^3
Pier elements	EI (kN m^2)	39,806,550
	ρA (kg m)	17,325
RHS abutment elements	EI (kN m^2)	1,062,600
	ρA (kg m)	4.241×10^3
Abutment pile elements	EI (kN m^2)	2.2266×10^6
	ρA (kg m)	6.7858×10^3
Pier pile elements	EI (kN m^2)	4.3488×10^6
	ρA (kg m)	8.4823×10^3

$$\mathbf{K_b} = \begin{bmatrix} \dfrac{EA}{L} & 0 & 0 & -\dfrac{EA}{L} & 0 & 0 \\[2mm] \vdots & \dfrac{12EI}{L^3} & \dfrac{6EI}{L^2} & 0 & -\dfrac{12EI}{L^3} & \dfrac{6EI}{L^2} \\[2mm] \vdots & & \dfrac{4EI}{L} & 0 & -\dfrac{6EI}{L^2} & \dfrac{2EI}{L} \\[2mm] \vdots & & \ddots & \dfrac{EA}{L} & 0 & 0 \\[2mm] \vdots & \ddots & & & \dfrac{12EI}{L^3} & -\dfrac{6EI}{L^2} \\[2mm] \ddots & \cdots & \cdots & \cdots & \cdots & \dfrac{4EI}{L} \end{bmatrix}$$

(1a)

Euler–Bernoulli frame elements, see [23]; the consistent mass $\mathbf{M_b}$ and stiffness $\mathbf{K_b}$ formulations for the elements are shown in Eqs. (1a, 1b). These matrices are symmetrical about the diagonal running top left to bottom right.

$$\mathbf{M_b} = \frac{\rho \mathrm{AL}}{420} \begin{bmatrix} 140 & 0 & 0 & 70 & 0 & 0 \\ \vdots & 156 & 22L & 0 & 54 & -13L \\ \vdots & & 4L^2 & 0 & 13L & -3L^2 \\ \vdots & & \ddots & 140 & 0 & 0 \\ \vdots & \ddots & & & 156 & -22L \\ \ddots & \cdots & \cdots & \cdots & \cdots & 4L^2 \end{bmatrix}$$
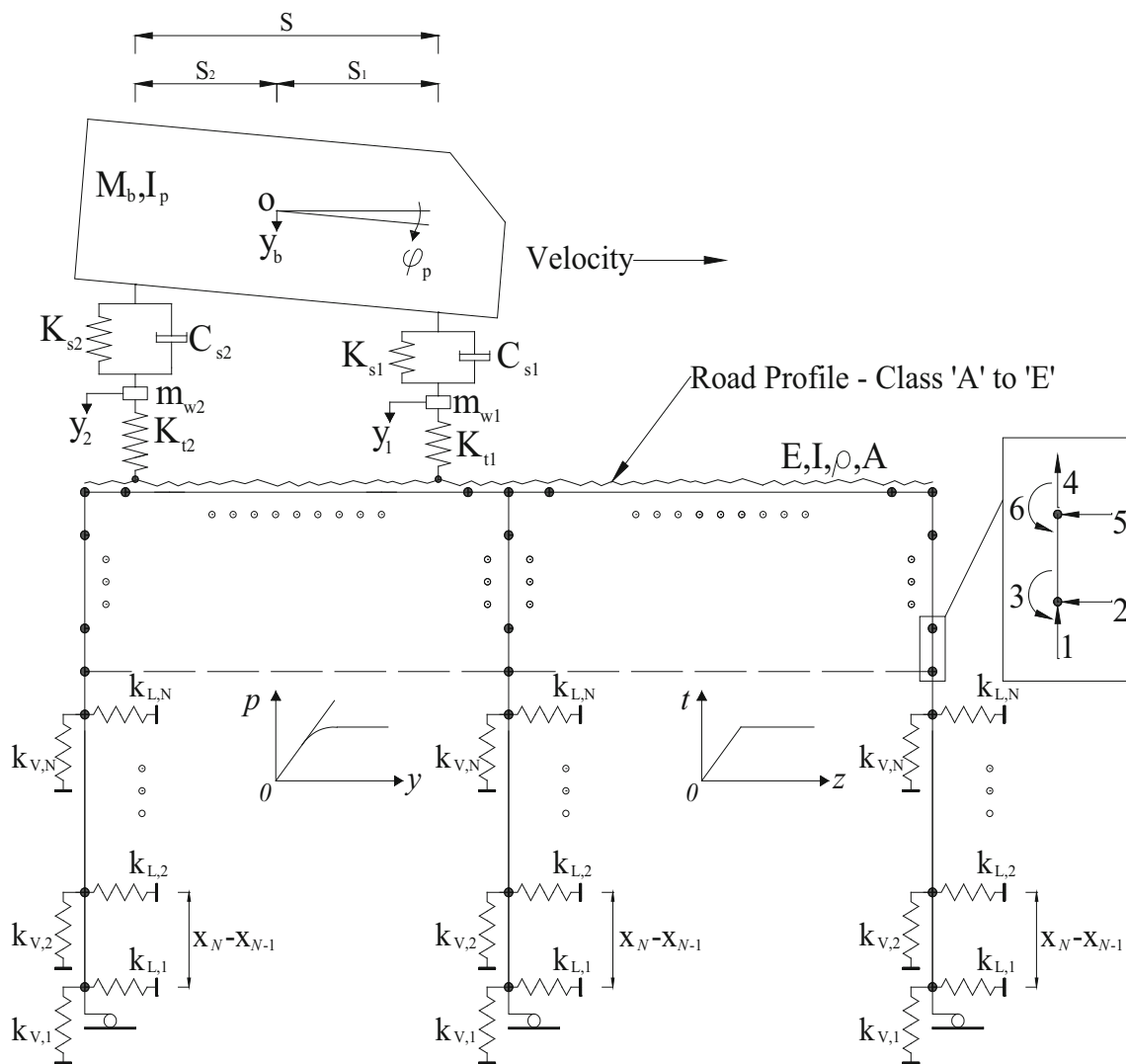
(1b)

Fig. 2 Schematic of numerical model used in simulations

where E is the Young's modulus of the material (N m^{-2}), I is the moment of inertia (m^4), A is the cross-sectional area (m^2), L is the length of the element (m), and ρ is the density of the material (kg m^{-3}). Each frame element has two nodes, each with an axial, transverse and rotational DOF, see the insert in Fig. 2. The soil surrounding the foundation piles is modelled using a system of discrete, mutually independent, closely spaced spring elements, known as Winkler springs [13, 24–26]. Each spring has 2-DOFs and permits 1-D movement only along the spring axis. Both horizontal and vertical distributed springs are used to model the lateral and axial soil impedances, respectively. The soil stiffness apportioned to the individual springs is discussed in a subsequent section.

The various frame and spring elements are assembled together to create global mass and stiffness matrices to mathematically model the structural system, using the procedure outlined in [23]. The dynamic system can be represented by the second-order matrix differential equation shown in Eq. (2).

$$\mathbf{M_B}\ddot{\mathbf{x}}(t) + \mathbf{C_B}\dot{\mathbf{x}}(t) + \mathbf{K_B}\mathbf{x}(t) = \mathbf{F_B}(t) \tag{2}$$

where $\mathbf{M_B}$, $\mathbf{C_B}$ and $\mathbf{K_B}$ are the $n \times n$ global mass, damping and stiffness matrices for the global bridge system and $\mathbf{x}(t)$, $\dot{\mathbf{x}}(t)$ and $\ddot{\mathbf{x}}(t)$ are vectors describing the displacement, velocity and acceleration of each system DOF (at a given time step). In total, the un-scoured bridge model has $n = 861$ DOFs. The vector $\mathbf{F_B}(t)$ describes the external forces acting on each DOF for a given time step and is ultimately populated using data from the vehicle model described in a subsequent section. Equation (2) is solved using the Wilson-theta integration scheme, with $\theta = 1.4$ for model stability [27, 28]. The damping matrix $\mathbf{C_B}$ is formulated as a linear combination of the global mass and

stiffness matrices, using a Rayleigh damping approach [29], as shown in Eq. (3).

$$\mathbf{C_B} = \alpha_0 \mathbf{M_B} + \alpha_1 \mathbf{K_B} \tag{3}$$

where $\alpha_0 = 2\xi\omega_1\omega_2/(\omega_1 + \omega_2)$ and $\alpha_1 = 2\xi/(\omega_1 + \omega_2)$. ω_1 and ω_2 are the first and second circular frequencies of the system (rad s^{-1}) and $\xi_1 = \xi_2 = \xi$ is the damping ratio adopted. All simulations in this paper are undertaken with a damping ratio of 2% to simulate energy dissipation from the system, which is broadly in keeping with the expected value for lightly damped structures and is broadly in line with the results obtained from pile tests presented in [26].

The undamped natural frequencies and mode shapes of the system can be determined by undertaking an eigenvalue analysis. For this, a system matrix $\mathbf{D_{SYS}}$ is specified, as shown in Eq. (4). The eigenvalues of $\mathbf{D_{SYS}}$ relate to the natural frequencies and the associated eigenvectors relate to the mode shapes, and are determined using an in-built eigen-function in MATLAB.

$$\mathbf{D_{SYS}} = \mathbf{M_B^{-1}} \mathbf{K_B} \tag{4}$$

2.2 Soil–structure interaction

The soil is modelled using Winkler springs [24] with stiffness corresponding to a uniform medium dense sand (see [16] for a study on soil density effects). The method for deriving spring stiffness coefficients is from the American Petroleum Institute [30, 31] design code, which specifies nonlinear relations for spring stiffness with strain. For the present paper, small-strain behaviour is assumed so the initial linear stiffness is adopted for each case. Specific details on how to calculate the lateral, Eq. (7) and vertical, Eq. (10) spring stiffnesses are given below.

2.2.1 Lateral soil stiffness

The lateral (horizontal) soil response is characterised by a set of soil reaction–lateral displacement (p–y) curves. The hyperbolic p–y formulation for sand as specified in the API design code [30] is shown in Eq. (5).

$$p = Ap_u \tanh\left(\frac{kx}{Ap_u} y\right) \tag{5}$$

where p_u is the ultimate resistance at depth 'x' below the ground surface (kN m^{-1}), k is the constant coefficient of subgrade reaction (kN m^{-3}), A is an empirical factor accounting for static or cyclic external loading, y is the lateral deflection (m). Numeric values for k are specified in the API design code [30]. k depends on the soil density (or friction angle) and varies for saturated and unsaturated conditions.

Equation (5) describes the nonlinear soil response over a large displacement (strain) range. The present paper is concerned with small amplitude dynamic loads applied to the foundation soil; therefore, it is assumed that the soil response will remain in the small-strain (linear) region. The initial stiffness k_{init} of the p–y curve can be obtained by differentiating Eq. (5) with respect to 'y', the lateral displacement as shown in Eq. (6).

$$k_{init} = \frac{\mathbf{d}p}{\mathbf{d}y}\Big|_{y=0} = Ap_u \frac{\frac{kx}{Ap_u}}{\cosh^2\left(\frac{kxy}{Ap_u}\right)}\Big|_{y=0} = kx \tag{6}$$

The depth-dependant modulus term (k_{init}) in Eq. (6) measured in units of kN m^{-2} can be converted to discrete spring stiffness moduli $k_{L,i}$ (kN m^{-1}) by multiplying by the spacing between springs at each spring depth, see Eq. (7).

$$k_{L,i} = k_{init}(x_N - x_{N-1}) \tag{7}$$

2.2.2 Vertical soil stiffness

The vertical soil stiffness against the pile shaft is characterised by a set of shear stress–vertical displacement (t–z) curves distributed along the shaft. Generic properties corresponding to a uniform medium dense sand are adopted. The load transfer t–z curves are developed based on the American Petroleum Institute [31] for sand which is formulated as shown in Eq. (8), whereby the ultimate soil resistance is assumed to be mobilised at a set displacement of 0.00254 m (converted from inches).

$$t/t_{max} = \begin{cases} 0, & z = 0\,\text{m} \\ 1, & z \geq 0.00254\,\text{m} \\ \dfrac{1}{0.00254}z, & 0 < z < 0.00254\,\text{m} \end{cases} \tag{8}$$

where t/t_{max} is the ratio of mobilised shear stress (kPa) to the ultimate shear resistance (kPa), which can be calculated using Eq. (9) [31].

$$t_{max} = K_L p_0' \tan\delta \tag{9}$$

where K_L is the coefficient of lateral earth pressure (assumed equal to 1 for full displacement piles), p_0' is the effective overburden pressure at the depth of the spring (kPa), δ is the friction angle between the soil and the pile shaft, taken as 25° for medium dense sand against concrete. The sand deposit is assumed to be normally consolidated with an effective unit weight of $\gamma' = 9$ kN m^{-3}. The linear vertical spring stiffness response can be obtained as the slope of the $t - z$ curve between $z = 0$ and $z = 0.00254$ m. Individual spring moduli (in units of kN m^{-1}) can then be obtained by multiplying the t_{max} value at a given depth by the shear area ($A_{s,i}$) over which each spring acts to convert this to a force value, see Eq. (10).

The shear area is the total combined discretised surface area of all the piles in the pile group over which each vertical spring acts.

$$k_{V,i} = \left(\frac{\mathbf{d}t}{\mathbf{d}z}\right)_i = \frac{t_{max,i}}{0.00254} \times A_{s,i} \qquad (10)$$

It is assumed that under vehicular loading, no load transfers to the pile base and the base is modelled as fully restrained in the vertical direction. This simplification had limited effect on the results.

2.3 Vehicle bridge interaction (VBI)

The bridge is loaded by a 15 tonne two-axle commercial truck (sprung 2-axle model) that traverses the bridge deck. The model used in this study is similar to the model used in [16, 21, 32, 33] and is intended to be representative of the kind of 2 axle trucks present in modern traffic fleets (i.e. it is not a special test vehicle). The purpose of using a representative truck model is to see if a standard vehicle can generate sufficient excitation of the relevant bridge modes. Figure 2 shows that the vehicle has four DOFs, namely a vertical body bounce (y_b), a body pitch (f_φ), front and rear axle hops (y_1 and y_2). The body of the vehicle is supported on a suspension/axle assembly and has mass m_b and rotational inertia I_p. Each axle/suspension assembly has a mass m_{w1} and m_{w2} for the front and rear axles, respectively. The suspension system for each axle has a stiffness coefficient K_{s1} and K_{s2} and a damping coefficient C_{s1} and C_{s2} for the front and rear assemblies, respectively. Finally, the front and rear tyres are modelled using linear springs with stiffness K_{t1} and K_{t2}, respectively. The equations of motion for the vehicle can be obtained by imposing equilibrium of all the forces and moments acting on the vehicle masses and expressing in terms of the system DOFs, allowing for vehicle mass $\mathbf{M_v}$, stiffness $\mathbf{K_v}$ and damping $\mathbf{C_v}$ matrices to be populated. The natural frequencies for the vehicle can be obtained by performing an eigenvalue analysis on the vehicle system matrix ($\mathbf{M_v^{-1}} \mathbf{K_v}$). Using the vehicle properties outlined in Table 2, these natural frequencies were determined to be 1.43, 2.07, 8.86, and 10.22 Hz for body bounce, pitch, front and rear axle hops, respectively. Note, changing the vehicle properties to model a different class of truck does not have a significant effect on the method, see [16].

The vehicle and bridge models interact dynamically via the contact forces that exist between the bridge deck surface and the vehicle wheels in a coupled and time-dependant problem [29]. It is necessary to solve both systems separately while maintaining compatibility at the contact points [34]. There are several approaches for undertaking analyses of this type and in this paper, an iterative approach was utilised to model the VBI [35, 36].

In all simulations, the vehicle commences motion at a distance of 100 m from the start of the bridge (approach length), so that the initial displacement $\mathbf{x_V}(t)$, velocity $\dot{\mathbf{x}}_V(t)$ and acceleration $\ddot{\mathbf{x}}_V(t)$ of the vehicle DOFs are realistic when the vehicle reaches the bridge. Vectors $\mathbf{x_V}(t)$, $\dot{\mathbf{x}}_V(t)$ and $\ddot{\mathbf{x}}_V(t)$ of the various vehicle DOFs are calculated by solving Eq. (11) using the Wilson-theta method [27].

$$\mathbf{M_V}\ddot{\mathbf{x}}_V(t) + \mathbf{C_V}\dot{\mathbf{x}}_V(t) + \mathbf{K_V}\mathbf{x_V}(t) = \mathbf{F_V}(t) \qquad (11)$$

where $\mathbf{F_V}(t)$ describes the external forces acting on the vehicle DOFs and primarily comprises the static weights of the axles and the body with variations due to the displacement of the tyre springs as it traverses the road surface and the motion of the body/axle assembly. These contact forces in $\mathbf{F_V}(t)$ are then used to populate the force vector $\mathbf{F_B}(t)$ of the bridge model, see Eq. (2). Equation (2) is solved to obtain the bridge response due to the vehicle forces and the vehicle and bridge responses are iteratively solved until convergence is achieved [35]. Convergence is deemed to have occurred when the largest difference in bridge displacement between the previous and current iterations is less than 1% of the largest current bridge displacement (bridge degree of freedom).

One of the primary variables that can affect the quality of a vibration signal is the condition of the road surface experienced by a traversing vehicle. Road surface topographies range from ISO Class 'A' (very good) to ISO Class 'E' (very poor) and these can be generated as per [37]. Road surface condition was observed not to significantly affect the method presented in this paper, which is based on frequency measurements; therefore, a Class 'A' profile (see Fig. 3) was adopted for all simulations (see Prendergast et al. [16] for a study on the effect of 'B' and 'C' class profiles).

3 Eigen analysis on the impact of scour at different locations

Before analysing acceleration signals from different locations on the bridge, it is first necessary to investigate how scour at different locations of a bridge substructure affects the vibration characteristics of the structure. Scour is simulated in the model by removing lateral and vertical springs (in pairs) sequentially commencing with those nearest the top of the foundation element under investigation. As the model is a 2-D frame, scour is assumed to occur along the full transverse length of a given support. The scour locations simulated are as follows, location A: 5 m deep scour hole at the LHS abutment; location B: 5 m

Table 2 Parameters of vehicle model

Parameter	Property	Value
Dimensions (m)	Wheel base (S)	5.5
	Dist from centre of mass to front axle (S_1)	3.66
	Dist from centre of mass to rear axle (S_2)	1.84
Mass (kg)	Front wheel/axle mass (m_{w1})	700
	Rear wheel/axle mass (m_{w2})	1100
	Sprung body mass (m_b)	13,300
Inertia (kg m^2)	Pitch moment of inertia of truck (I_p)	41,008
Spring stiffness (kN m^{-1})	Front axle (K_{s1})	400
	Rear axle (K_{s2})	1000
Damping (kN s m^{-1})	Front axle (C_{s1})	10
	Rear axle (C_{s2})	10
Tyre stiffness (kN m^{-1})	Front axle (K_{t1})	1750
	Rear axle (K_{t2})	3500

Fig. 3 Road roughness profile—Class 'A'
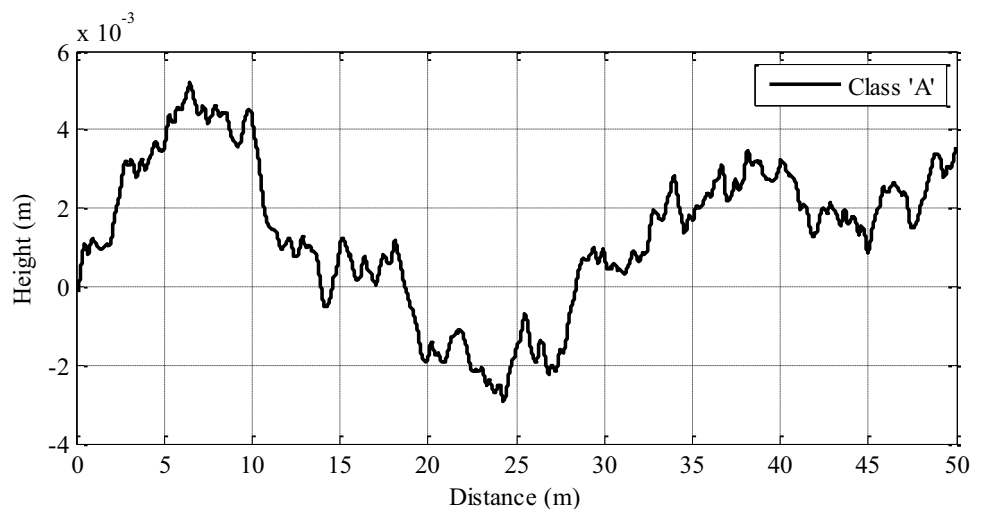
deep scour hole at the pier; location C: 5 m deep scour hole at the RHS abutment and location D: 5 m deep scour hole across all foundations, see Table 3.

The choice of 5 m scour stems from Prendergast et al. [16] which investigated the frequency change observed as scour increased in severity from 0 to 10 m so in this paper, which presents a scour location technique, the median value from the previous work is used. The reason for modelling just one scour depth is that the focus of this paper is on identifying scour location rather than tracking the shift in frequencies observed due to gradual scouring of the bridge. 5 m scour equates to the removal of 10 spring-pairs from around the foundation element under investigation. The scour condition is maintained constant at either

zero scour or 5 m scour to study the effects on the Eigen frequencies of the bridge. Un-scoured mode shapes for the first six vibration modes of the bridge and the changes in frequency observed for the different scour locations are reported below.

3.1 Un-scoured theoretical mode shapes

The theoretical mode shapes and frequencies for the first six modes of the un-scoured bridge are shown in Fig. 4. Figure 4a shows a global sway mode, termed M1. Figure 4b shows predominately a deck mode, termed M2. Figure 4c shows also predominately a deck mode, termed M3. Figure 4d shows predominately an LHS abutment

Table 3 Scour locations

Location A	Location B	Location C	Location D
5 m scour LHS abutment	5 m scour central pier	5 m scour RHS abutment	5 m scour all foundations

mode, termed M4. Figure 4e shows predominately an RHS abutment mode, termed M5 and finally Fig. 4f shows predominately a pier mode, termed M6. M1 acts as a global mode for the structure whereas the remaining modes 2–6 act in a predominately local fashion, i.e. most of the movement occurs within an individual element [17]. The change in frequency observed when scour is applied at locations A–D is investigated in the next section.

3.2 Effect of scour location on Eigen frequencies

The effect of applying the scour scenarios (shown in Table 3) on modes M1–M6 (frequencies) is shown in Table 4. The zero scour modal frequencies are displayed in the first row and correspond to the mode shapes shown in Fig. 4. By examining the first column of Table 4, it can be seen that M1, the global sway mode, is most sensitive to scour of the central pier (Location B, with frequency changing from 1.43 to 1.135 Hz) and scour across all foundations (Location D, with frequency changing from 1.43 to 0.989 Hz). By examining the relevant columns of Table 4, it can be seen that M2 and M3, which are predominately deck modes, are relatively unaffected by scour of the foundations with only minor frequency changes

occurring. This finding is similar to the results presented in [20]. M4 is a local mode and only experiences frequency changes for scour affecting the LHS abutment, namely location A (LHS scour) and location D (all scour). It is unaffected by scour at other locations. Similarly, M5 and M6 act in the same way in the sense that they only show a change in frequency if there is scour local to the element. For example, M5 is only affected by scour of the RHS abutment, namely location C (RHS scour) and location D (all scour). M6 is only affected by scour of the pier, namely location B (pier scour) and location D (all scour) and is relatively unaffected by scour elsewhere.

The results in Table 4 are more effectively shown as the percentage change in frequency from the zero scour case for each scour location, see Fig. 5. For each scour location (A–D), the resulting percentage change in each modal frequency is plotted. The results show that applying scour location A (LHS abutment scour) mainly affects M4 and M1 with percentage changes in frequency of 31.1 and 3.97%, respectively. Applying scour at location B (pier scour) predominately affects M1 and M6, with percentage changes in frequency of 20.65 and 14.36% occurring. The large change in M1 due to pier scour can be understood by the fact that the pier provides the bulk of the bridge's

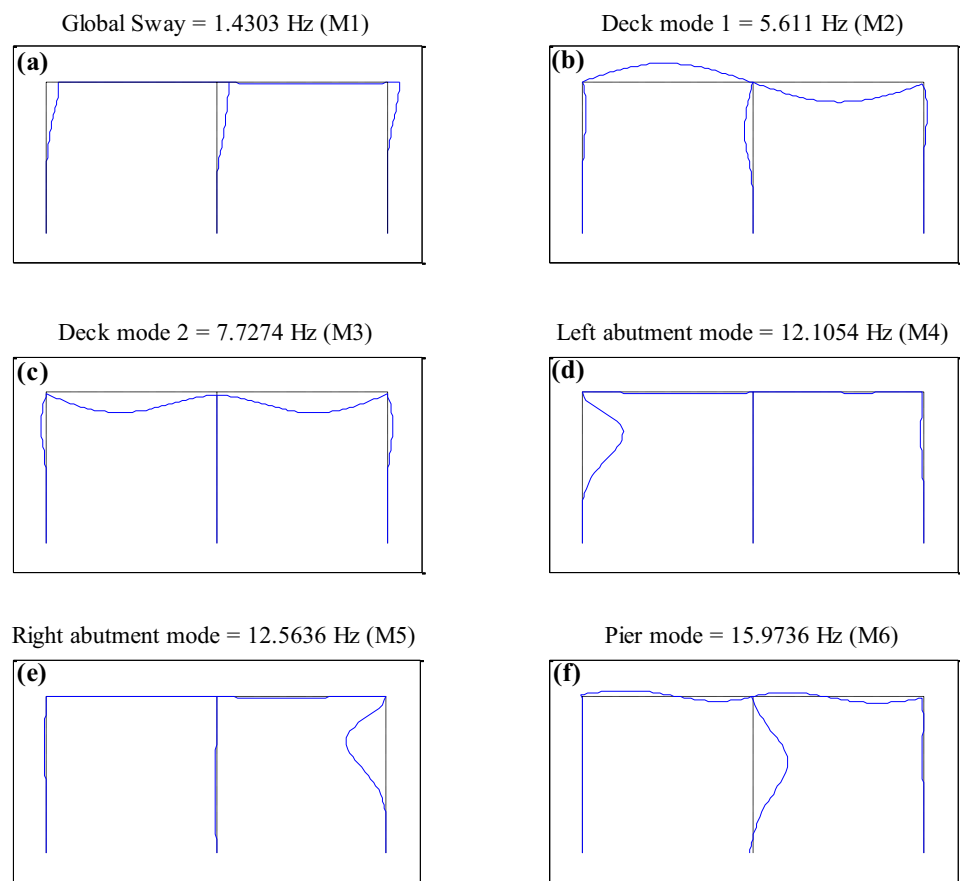**Fig. 4** Un-scoured theoretical mode shapes. **a** M1, **b** M2, **c** M3, **d** M4, **e** M5, **f** M6

Global Sway = 1.4303 Hz (M1)

(a)

Deck mode 1 = 5.611 Hz (M2)

(b)

Deck mode 2 = 7.7274 Hz (M3)

(c)

Left abutment mode = 12.1054 Hz (M4)

(d)

Right abutment mode = 12.5636 Hz (M5)

(e)

Pier mode = 15.9736 Hz (M6)

(f)

Table 4 Scour effect on modal frequencies

Scour location	M1 (Hz)	M2 (Hz)	M3 (Hz)	M4 (Hz)	M5 (Hz)	M6 (Hz)
Zero scour	1.43	5.611	7.727	12.105	12.564	15.974
5 m scour LHS (A)	1.374	5.6	7.652	8.34	12.562	15.971
5 m scour pier (B)	1.135	5.46	7.716	12.105	12.563	13.68
5 m scour RHS (C)	1.369	5.599	7.67	12.108	8.6634	15.971
5 m scour all (D)	0.989	5.434	7.589	8.335	8.6624	13.678
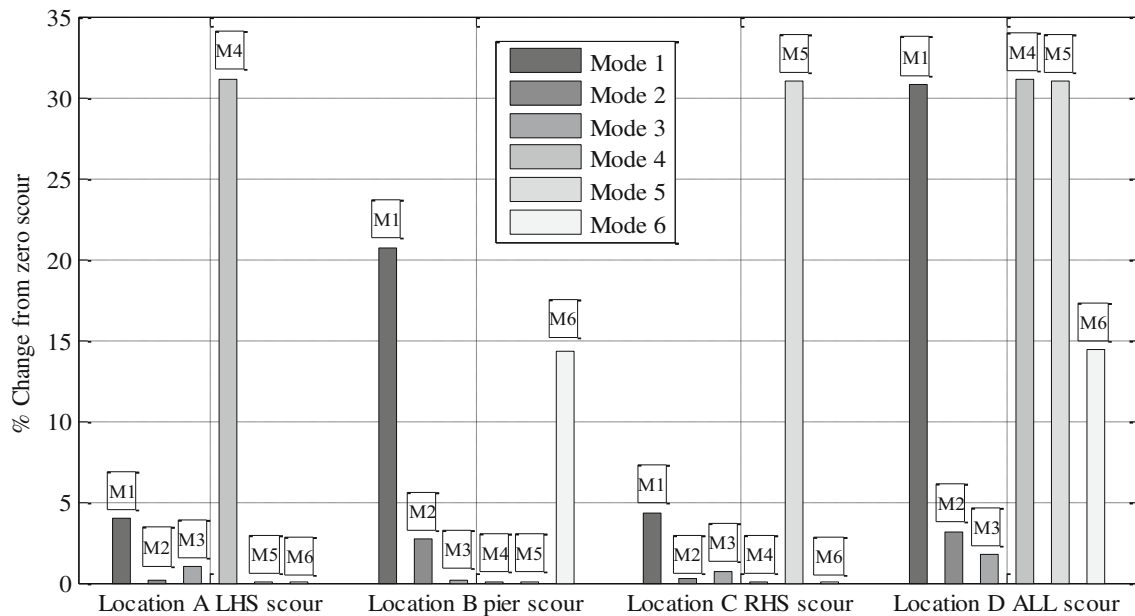
Fig. 5 Percentage change in natural frequency of the first six modes for four different cases of scour; *Location A* 5 m scour left abutment, *Location B* 5 m scour central pier, *Location C* 5 m scour right abutment, *Location D* 5 m scour to left abutment, central pier and right abutment

longitudinal stiffness, and scour at this location will have a significant effect on frequency. Applying scour location C (RHS abutment scour) predominately affects M1 and M5 with percentage changes of 4.3 and 31%, respectively. Scour location D (5 m scour across all foundations) has a major effect on M1, M4, M5 and M6 with percentage changes of 30.8, 31, 31, and 14%, respectively.

From Fig. 5, one can observe that certain modes experience a change in frequency irrespective of where scour occurs, e.g. M1 shows some change in frequency for scour locations A–D. However, other modes only show changes in frequency for specific scour locations, e.g. M4 only shows a change if the scour occurs at the LHS abutment. Similarly, M5 only shows a change in frequency if the scour occurs at the RHS abutment. This predominately local behaviour of M4, M5 and M6 means that observing changes in these modes may potentially be used to locate a scour hole affecting a structure. For example if there is a shift in the frequency of M4, it indicates that there may be scour specifically at the LHS abutment. To track these frequency changes on a real bridge will require the analysis

of time-domain acceleration signals arising on the structure and the feasibility of doing this is investigated in the next section.

4 Detecting the location of scour by analysing acceleration signals from VBSI model

In the previous section, an eigenvalue modal analysis was conducted to investigate how scour at different locations affects the modal frequencies of an integral bridge structure. This analysis showed that M4, M5 and M6 were affected predominately by scour occurring at the LHS abutment, RHS abutment and pier, respectively, and were relatively unaffected by scour elsewhere. On a real bridge, it is not possible to undertake an eigenvalue analysis. Instead, it is necessary to collect dynamic signals and analyse them for their frequency content. Obviously bridge vibration can be excited by a number of external sources, e.g. traffic, wind, and other factors. Farrar et al. [38] present a literature review on different methods to excite

highway bridges for modal testing. They report that while using vehicle loading to excite the structure has its disadvantages (e.g. vehicle vibrations appearing in the bridge response) in many cases using ambient vibrations resulting from vehicle vibrations is the only practicable way of exciting the structure. Therefore, this section investigates if it is practicable to locate scour affecting a structure by analysing accelerations arising when the structure is excited by vehicle loading. To make the simulations as realistic as possible, VBI effects are included. Optimum locations to distribute sensors on the structure to capture the required modal information, signal processing required to track bridge frequencies and determining the location of a scour hole based on the analysis of response signals are subsequently presented. The effect of (added) sensor noise on the resilience of the approach is also investigated.

4.1 Optimum sensor placement to detect bridge frequencies based on mode shapes

Based on the eigenvalue modal analysis and the mode shapes shown in Fig. 4, the minimum number of sensors required to effectively analyse the structural response is four sensors, S1–S4, distributed as shown in Fig. 6. Sensors are positioned close to the anti-nodes of the scour sensitive modes, i.e. M1 should be detected from sensor S2, M4 from S1, M5 from S3 and M6 from S4. Since M2 and M3 are not sensitive to scour, these are not targeted in this analysis. Note, in reality to identify appropriate sensor locations and number of sensors required for a given bridge it will be necessary to undertake Eigen analyses such as that shown in Fig. 4 (i.e. an FE model will be required) and/or carry out experimental modal testing on the bridge.

4.2 Signal processing of bridge acceleration signals to track frequency

To visualise the bridge response as detected at S1–S4 due to a passing vehicle, a simulation is carried out where a vehicle traverses the bridge at 30 km h^{-1}. The vehicle is a two-axle truck (see Table 2 for properties) and traverses a Class 'A' road surface (see Fig. 3). No scour is implemented in this simulation. The results are shown in Fig. 7.

Figure 7a shows the lateral bridge displacement response due to the vehicle traversing. The bridge undergoes global sway to the left (negative displacement) while the vehicle is on the LHS span (between $t = 0$ s and $t = 3.3$ s), then undergoes sway to the right (positive displacement) while the vehicle traverses the RHS span (between $t = 3.3$ s and $t = 6.6$ s). The lateral acceleration signals detected at the abutment sensors (S1 and S3) are shown in Fig. 7b and at the pier sensors (S2 and S4) are shown in Fig. 7c. A total of three impulses can be seen, Fig. 7b, corresponding to the vehicle front and rear axles entering and the front axle leaving the bridge. As this paper is concerned with locating a scour hole by observing the frequency content of distributed sensors, the acceleration signals generated at each sensor location are analysed herein.

Figure 8 shows the frequency content of the acceleration signals in Fig. 7b, c, obtained by passing the signals though a fast Fourier transform algorithm. This is achieved in MATLAB using an in-built Fourier Transform algorithm. Figure 8a shows the frequency spectra of the acceleration signals from abutment sensors S1 and S3. Also shown are the location of the Eigen frequencies annotated M1 to M6. This figure shows that a series of peaks are detected between M3 and M5. Figure 8b shows the frequency content of the pier top sensor S2, with a dominant peak at M1 being clearly detected and a minor peak at M2. Figure 8c shows the frequency content of the lower pier sensor S4. A series of peaks are detected in the vicinity of M6 with minor peaks elsewhere. These data show that the frequency spectra from the 'sensors' are quite noisy. In particular, the peaks between M3 and M5 in Fig. 8a occur due to interaction effects between the vehicle and the road profile. To highlight this, Fig. 8d shows the frequency content obtained from the acceleration signal at S1 when the vehicle traverses a 'smooth' road surface, in lieu of the Class 'A' surface. In this plot, the frequency response appears smoother and M3 and M4 can be clearly detected with smaller peaks between them. It is noteworthy that these smaller peaks most likely correspond to the axle frequencies of the vehicle, which are 8.86 and 10.22 Hz for the front and rear axles, respectively. The analysis conducted in Figs. 7 and 8 shows that the frequency content of
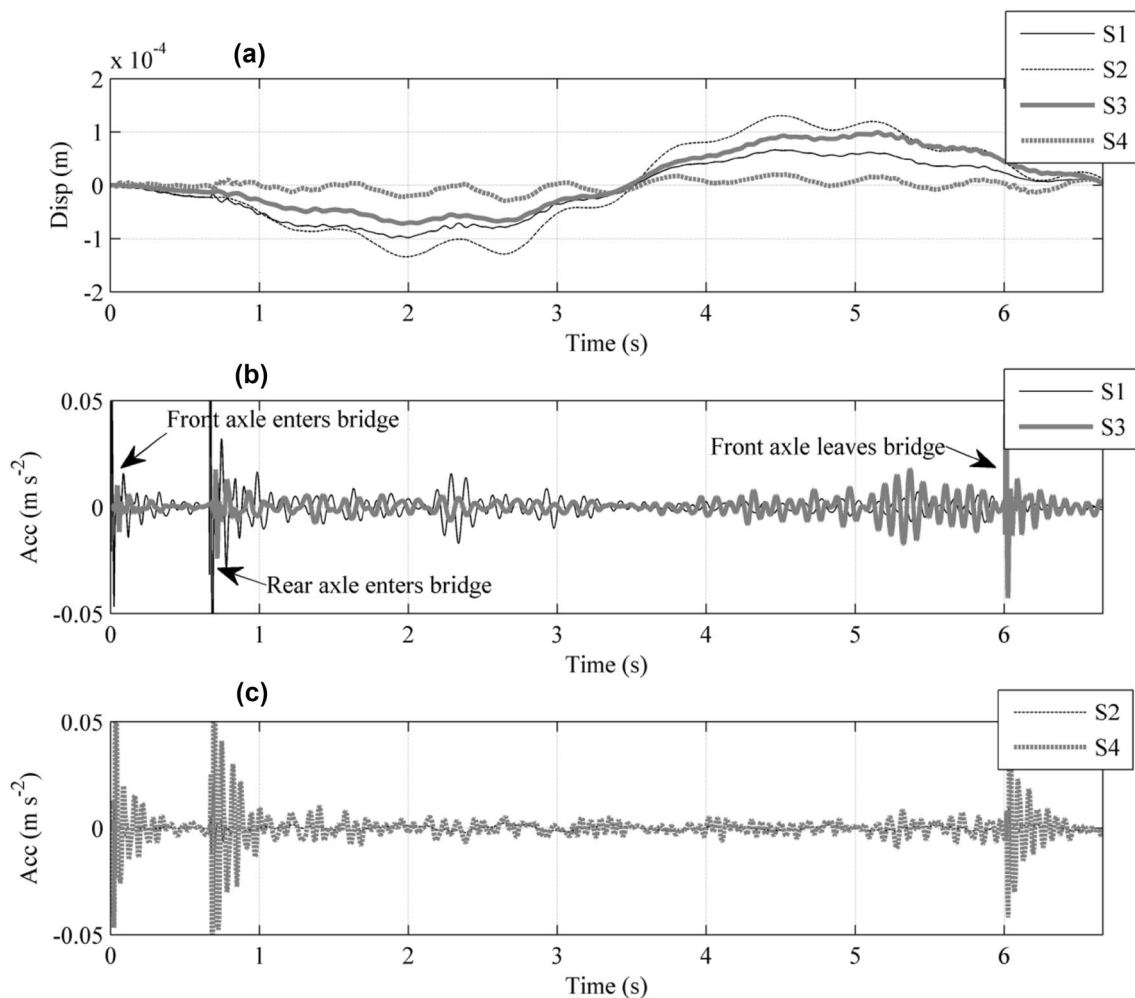

Fig. 6 Sensor distribution on superstructure
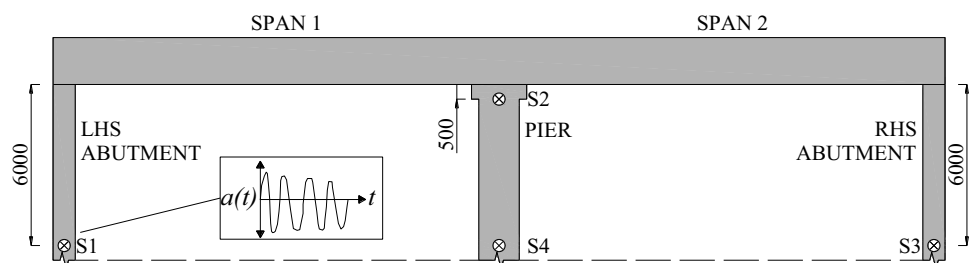
Fig. 7 Displacement and acceleration signals from sensors S1 to S4 due to passage of vehicle at 30 km h^{-1} over a Class 'A' profile. **a** Lateral displacement response sensors S1–S4; **b** lateral acceleration responses at sensors S1 and S3 on each abutment; **c** lateral acceleration responses at sensors S2 and S4 on the pier

the accelerations generated due to vehicular loading is generally quite noisy. With the exception of S2 (Fig. 8b), it would be difficult for a bridge manager to track bridge frequencies using raw acceleration data arising from vehicular loading alone. The clarity of the frequency response would also be quite sensitive to the vehicle velocity since a higher vehicle speed leads to a shorter signal available for analysis, which has knock-on effects for frequency resolution. In Fig. 8, the vehicle traversed the bridge at 30 km h^{-1}.

In Fig. 9a–c, the acceleration signal measured at S2 is analysed for its frequency content for three different vehicle speeds; 30, 60, and 100 km h^{-1} over a Class 'A' road profile, in order to investigate the effect of vehicle velocity on the clarity of the frequency spectra. In Fig. 9d, frequency peaks are evident at locations close to M1 and M2, inserts (e) and (f) on the figure show zoomed in views of these regions. Increasing the speed of the vehicle has the

effect of shortening the forced vibration in the time domain (see Fig. 9a–c). This has the knock on effect of reducing the frequency resolution for increased speed, note the larger distance between consecutive data points in inserts (e) and (f). This resolution for increasing speed leads to two difficulties: (1) even in the absence of scour the modal peak will appear at a slightly different frequency for each speed and, (2) even if every vehicle was travelling at 100 km h^{-1} it would be difficult to detect small changes in frequency due to scour because of the coarse frequency resolution. It is also evident that changing the vehicle velocity leads to a difference in the height of the frequency peak observed at M1 and M2, i.e. the different vehicle velocities leads to a variation in the excitation of modes 1 and 2 of the bridge. Moreover, extra frequency peaks to the left of M1 appear in the frequency spectra. This can be clearly seen for the 60 km h^{-1} case. The origin of these extra peaks is discussed subsequently.
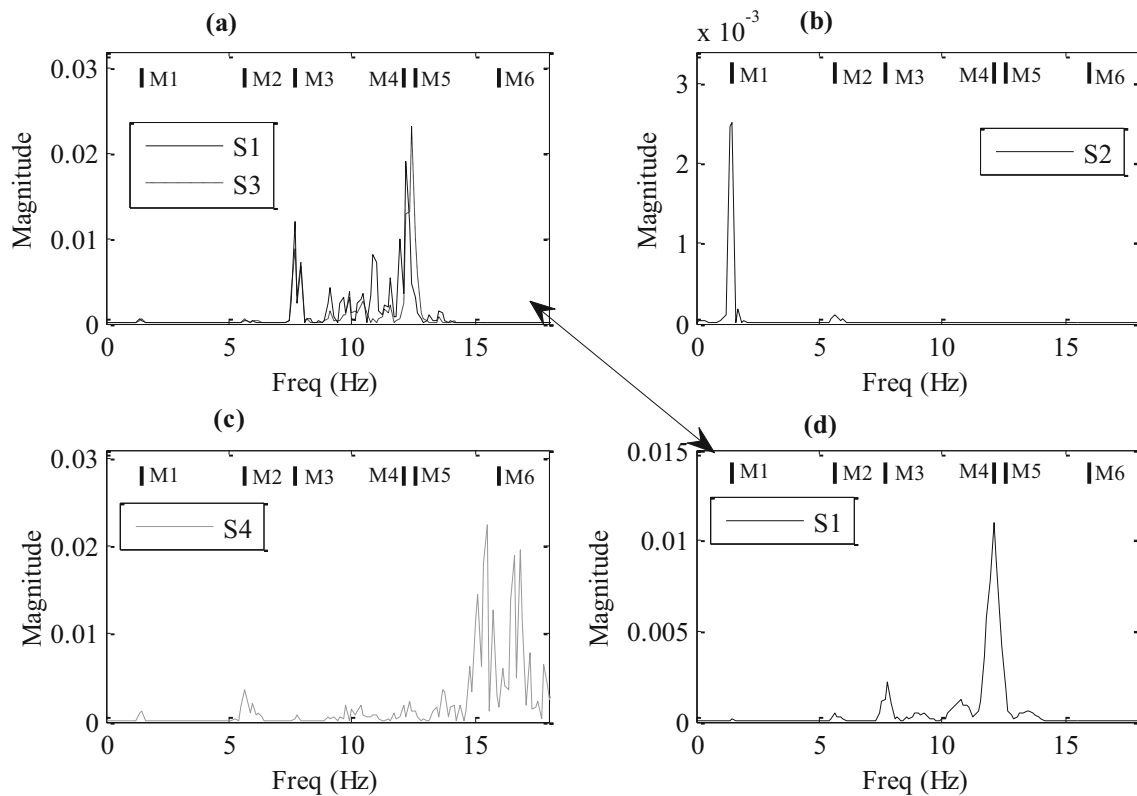
Fig. 8 Frequency content of accelerations signals from bridge sensors due to vehicle passage at 30 km h^{-1} over a Class 'A' profile. **a** Frequency content of sensors S1 and S3; **b** frequency content of sensor S2; **c** frequency content of sensor S4; **d** frequency content of sensors S1 in the absence of a road profile

It is evident from Fig. 9 that using only the forced vibration part of the signal will be problematic, i.e. in reality vehicles will cross at different speeds leading to different frequency resolution. Recognising that a bridge structure will continue to oscillate with damped free vibration after a vehicle has departed will increase the frequency resolution considerably. To identify an adequate signal length for analysis and to make use of free vibration, a datum frequency resolution is required. For this case, the required resolution is chosen as that which would be sufficient to detect a change in global sway frequency for a 1 m scour hole around the bridge pier, see [16]. A 1 m scour hole around the pier reduces the frequency of M1 from 1.43 to 1.3982 Hz, a difference of 0.032 Hz, as determined from an eigenvalue analysis. The minimum required signal length to give the required resolution is determined as 31.25 s, using a simple calculation relating frequency resolution to time length of signals. Note, on a real bridge any desired signal length can be used so long as it has sufficient length, the analysis undertaken in this paper is for demonstration purposes.

By including free vibration after the vehicle departs the bridge, it is possible to make the total length of the signal

32 s and the analysis from Fig. 9 can be revised, as shown in Fig. 10.

Figure 10a–c shows the acceleration signals measured at S2 for a vehicle traversing at 30, 60 and 100 km h^{-1} each with free vibration included. Once again, the vehicle traverses a Class 'A' road profile. Figure 10d shows the frequency content of the signals in Fig. 10a–c, with insert (e) showing zoomed in views of the region around M1. When Fig. 10d is compared to Fig. 9d, it can be seen that including free vibration improves frequency resolution with clear peaks detected at M1 and M2 for all velocities. Also evident, however, are the presence of unexpected peaks to the left of M1, at approx. 0.23, 0.47, and 0.885 Hz. These were also present in Fig. 9e also but are much clearer in this revised plot. These frequencies are essentially forcing (loading) frequencies, i.e. when the vehicle is on the left span, it causes the span to deflect downward inducing global sway movement to the left, and while it is on the right span, it induces global sway to the right. These frequencies are shown clearly in the insert Fig. 10e and increase for higher vehicle velocities. More information on the origin of these frequency peaks is available in [21].
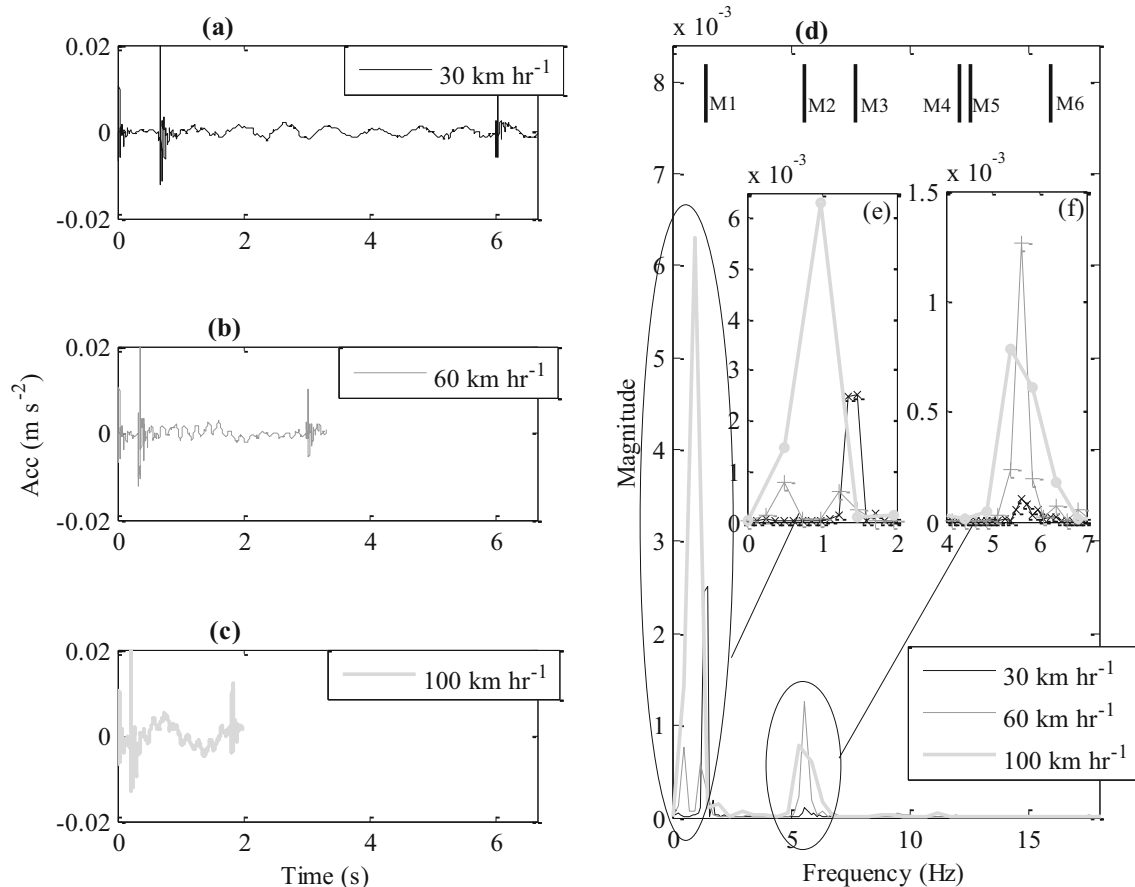
Fig. 9 Effect of vehicle velocity on frequency response of structure—sensor S2. **a** Acceleration measured due to vehicle traversing at 30 km h^{-1}; **b** acceleration measured due to vehicle traversing at 60 km h^{-1}; **c** acceleration measured due to vehicle traversing at 100 km h^{-1}; **d** frequency content of signals in (**a**–**c**)

The presence of vehicle loading frequencies in the spectrum of acceleration could potentially affect the ability for bridge frequencies to be accurately tracked, especially if the vehicle loading frequencies are close to the bridge frequency. In order to avoid this potential issue, analysing only the free vibration data after a vehicle has departed the bridge is implemented in Fig. 11. Figure 11a–c shows that the free vibration at S2 after the vehicle has departed the bridge for vehicle velocities of 30, 60 and 100 km h^{-1}, respectively. Figure 11d shows the frequency content of the signals in (a) to (c). In this figure, it can be seen that the vehicle loading frequencies have disappeared and that the frequencies of M1 and M2 are now clearly evident in the spectra for the three velocities. Using the free vibration signal after a vehicle departs the bridge would, therefore, seem to be a reliable way of detecting the frequency response of the bridge as it removes contributions associated with vehicle behaviour. Using free vibration data will also avoid the unwanted frequency peaks associated with the vehicle and the road profile that were evident in Fig. 8a

(particularly between M3 and M4). This pattern of having a 'cluttered' spectra (many frequency peaks) during the forced vibration and a cleaner spectra (fewer, but more clearly evident peaks) during free vibration is consistent with experimental work reported by Ülker-Kaustell and Karoumi [39] who analysed the vibration response of a bridge subject to train loading. Among other things, the authors showed (using wavelet analysis) the time varying nature of the frequencies during the forced response and also how the bridge frequencies were relatively easily identified when just the free vibration response was analysed.

4.3 Determining scour location based on response signals

In this section, analysing acceleration signals from different sensor locations as a means of locating a scour hole is investigated. From the eigenvalue analysis undertaken previously, it was determined that modes M4, M5 and M6
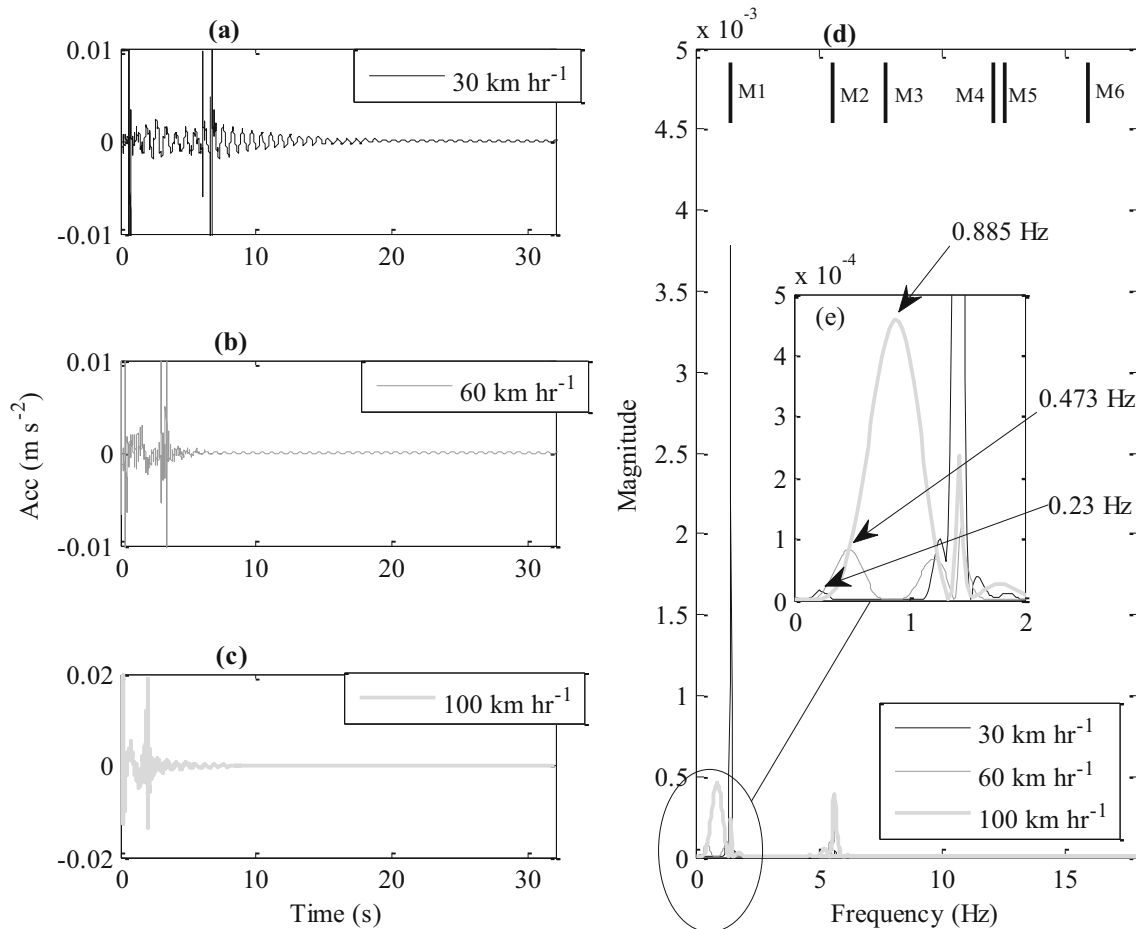
Fig. 10 Effect of vehicle velocity on frequency response of structure—sensor S2. **a** Acceleration measured due to vehicle traversing at 30 km h^{-1} + 30 s free; **b** acceleration measured due to vehicle traversing at 60 km h^{-1} + 30 s free; **c** acceleration measured due to vehicle traversing at 100 km h^{-1} + 30 s free; **d** frequency content of signals in (**a**–**c**)

act in a predominately local manner and only experience changes in frequency for scour affecting the LHS abutment, RHS abutment and pier, respectively. The purpose of this section is to ascertain if this property can be used to identify the location of scour. Initially, this is investigated by implementing 5 m scour at the LHS abutment (location A) and analysing the frequency shifts observed at various 'sensor' points. In all cases, the time series signals analysed are the free vibration following a vehicle traversing the bridge at 30 km h^{-1} and travelling on a Class 'A' road profile. The results of the simulation are summarised in Fig. 12. Figure 12a shows how the frequency content observed at S1 varies due to scour at the LHS abutment. The solid plot shows the frequency when there was zero scour and the dashed plot shows the frequency when there was 5 m scour at the LHS abutment. (Note, the solid and dashed plots are plotted with respect to the left and right axes, respectively, this was to accommodate some variation in the magnitude of the frequency peaks). For the case of zero scour (solid plot), frequencies of M1, M2, M3 and M4

are clearly detected in the spectrum with M5 and M6 not captured. This is sensible as by observing Fig. 4 it can be seen that modes M1–M4 exhibit some modal displacement at the location of sensor S1 (see Fig. 6), whereas M5 and M6 exhibit almost none. The dashed plot in Fig. 12a shows the frequency from S1 when there has been 5 m scour of the LHS abutment. By comparing the dashed plot to the solid plot it can be seen that the occurrence of scour at this location results in M1 frequency reducing from 1.434 to 1.373 Hz. M2 and M3 are still detected at approximately the same locations; however, M4 has experienced a large reduction in frequency from 12.08 to 8.21 Hz. This result is broadly in agreement with the results of the Eigen analysis shown in Table 4.

Figure 12b shows how the frequency content observed at sensor S2 on the pier head varies due to scour of the LHS abutment, with solid and dashed plots showing zero scour and 5 m scour, respectively. In this figure, M1 is clearly detected for the case of zero scour at 1.434 Hz (solid plot). When 5 m of LHS abutment scour is implemented, the
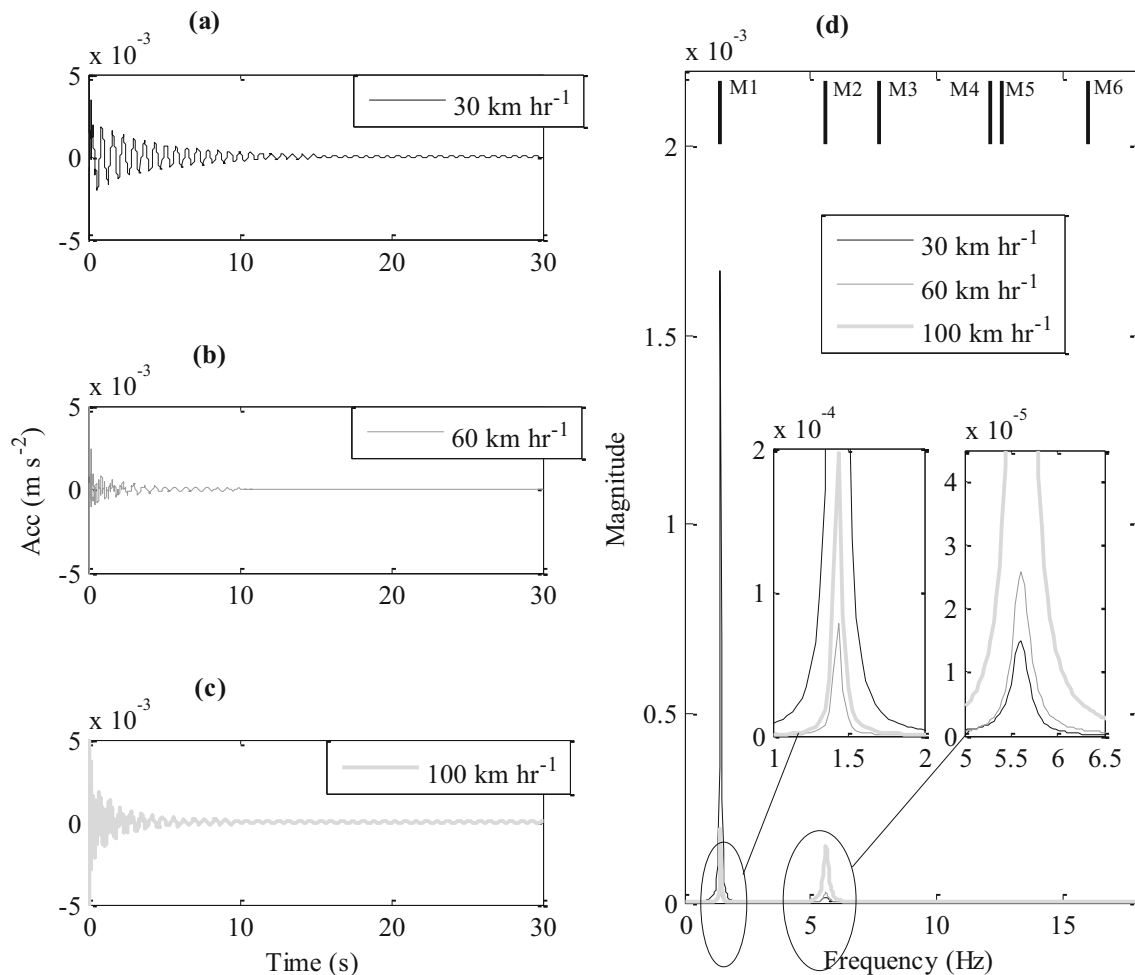
Fig. 11 Free vibration only– sensor S2. **a** Free vibration measured after vehicle traversed at 30 km h^{-1}; **b** free vibration measured after vehicle traversed at 60 km h^{-1}; **c** free vibration measured after vehicle traversed at 100 km h^{-1}; **d** frequency content of signals in (**a–c**)

peak frequency shifts to 1.373 Hz, which agrees with the change in M1 observed in Fig. 12a.

Figure 12c shows how the frequency content observed at sensor S3 on the RHS abutment varies due to scour of the LHS abutment. In this figure, it can be seen that for zero scour (solid plot) M1, M2, M3 and M5 are clearly detected in the frequency spectrum, with M4 and M6 not captured. For the scoured case (dashed), the same frequencies are identified. M1 shows a small change in frequency going from 1.434 to 1.373 Hz. For M2 and M3, no significant shift in frequency is observed. M5, the RHS abutment mode, is completely unaffected by scour of the LHS abutment, with the frequency remaining at 12.51 Hz before and after scour. Figure 12d shows the frequency data detected at sensor S4, on the lower pier. Modes M1, M2 and M6 are detected at this sensor location. Once again, only M1 experiences a change in frequency from 1.434 to 1.373 Hz with the remaining captured modes exhibiting little to no frequency change.

The results presented in Fig. 12 show that M4, M5 and M6 act as local modes, i.e. only the sensors on the respective elements are able to detect these frequencies. Moreover, it appears that the local mode of the element that has experienced scour (M4—LHS abutment, in this case) shows a very large shift in frequency (δM4) with the other local modes (M5 and M6) showing no change in frequency. The results of Fig. 12 are summarised in Fig. 13a.

In Fig. 13a, the percentage change in frequency (horizontal axis in Fig. 12) for a given mode (M1–M6) for a given sensor (S1–S4) is represented by a vertical column. For example in Fig. 12, it was observed that for sensors S1–S4 the frequency of M1 reduces from 1.434 to 1.373 Hz when there is scour of the LHS abutment (indicated as δM1 in Fig. 12a–d). This was a change in frequency of 4.25%. This change is presented as four equal height columns in the upper part of Fig. 13a. During the discussion of Fig. 12, it was also observed that the only other mode to show a significant
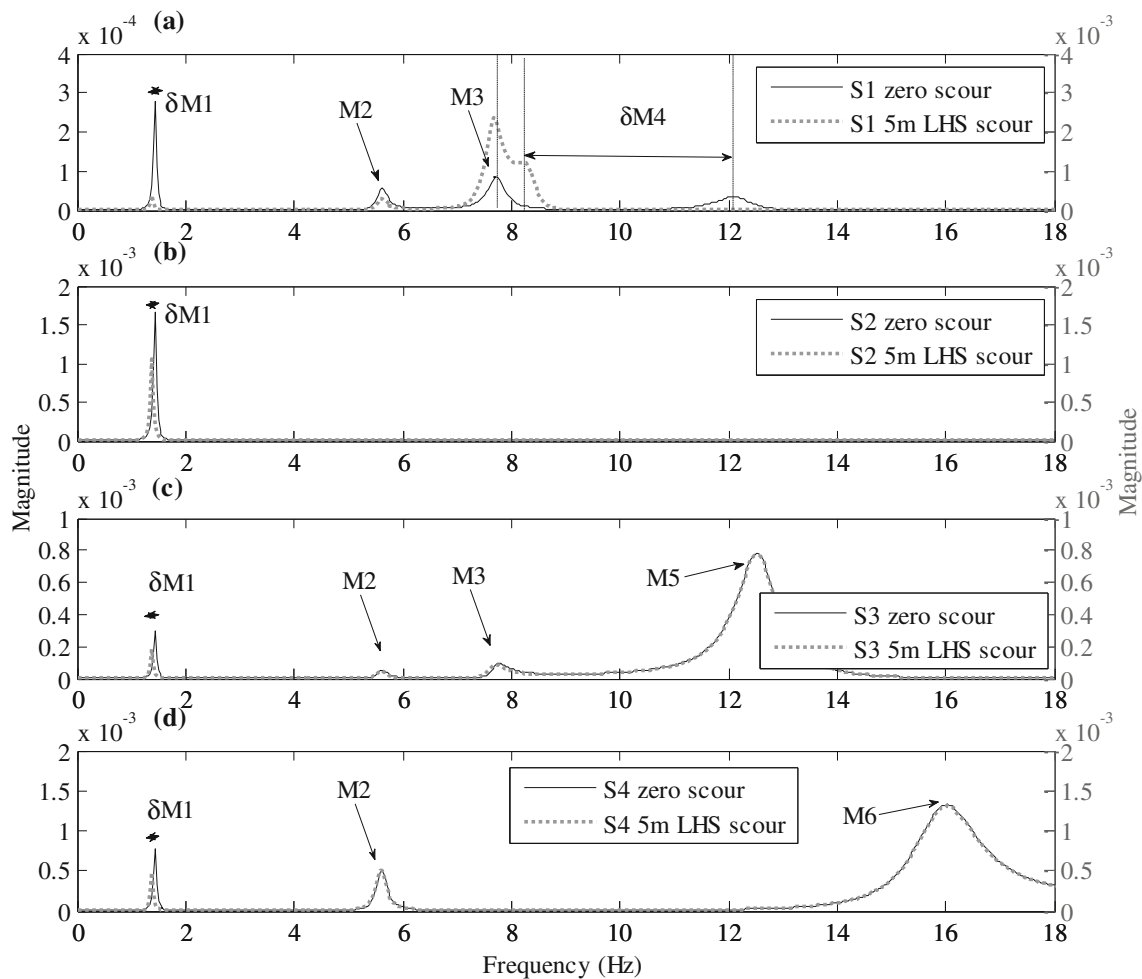
Fig. 12 Zero scour and 5 m LHS scour—Location A as detected by sensors S1, S2, S3 and S4—30 km h^{-1} vehicle speed—free vibration portion only **a** sensor S1 zero scour and 5 m LHS scour; **b** sensor S2 zero scour and 5 m LHS scour; **c** sensor S3 zero scour and 5 m LHS scour; **d** sensor S4 zero scour and 5 m LHS scour

frequency change was M4, which was found to reduce from 12.08 to 8.21 Hz (a 32% shift in frequency) and this change was only evident in sensor S1 data (Fig. 12a). This frequency change is represented by the tall black column in Fig. 13a. The rest of the columns in Fig. 13a are small or zero to represent the fact that during the examination of Fig. 12 other frequency shifts were negligible. Figure 13b presents the frequency changes observed when there is 5 m scour at the pier (location B). Similar to Fig. 13a, M1 shows the same percentage changes in frequency across all four sensors (S1–S4). However, the change in frequency for M1 (21%) is significantly larger than that observed in Fig. 13a. This is simply because the pier is significantly stiffer than the abutments so any scour experienced by the pier will have a larger impact on the frequency than an equivalent level of scour at the abutment. The other significant frequency change observed in Fig. 13b is for M2 and M6. M2 shows a percentage change in frequency of 2.7% and the same level of change is observed for all four sensors. M6 (local pier

mode) exhibits a change in frequency of 14.67% and the change can only be observed at S4 which is the sensor on the lower pier. This is consistent with the pattern observed in Fig. 13a, in the sense that only the sensor on the element which experienced scour will detect changes in the local vibrations of that element. Figure 13c shows the percentage change observed in the modal frequencies when there is 5 m scour of the RHS abutment. Not surprisingly the frequency changes observed are very similar to those observed for scour of the LHS abutment (Fig. 13a) in that all sensors identify the small frequency changes in M1 and only the sensor on the right hand side abutment (S3) identifies the change in the local mode M5. Finally, Fig. 13d shows the percentage change in the modal frequency observed when the pier and both abutments are scoured by 5 m. The percentage changes in frequency at each sensor as shown in Fig. 13d are effectively a summation/superposition of the equivalent changes in frequency in parts (a–c) of Fig. 13, allowing for some numerical errors.
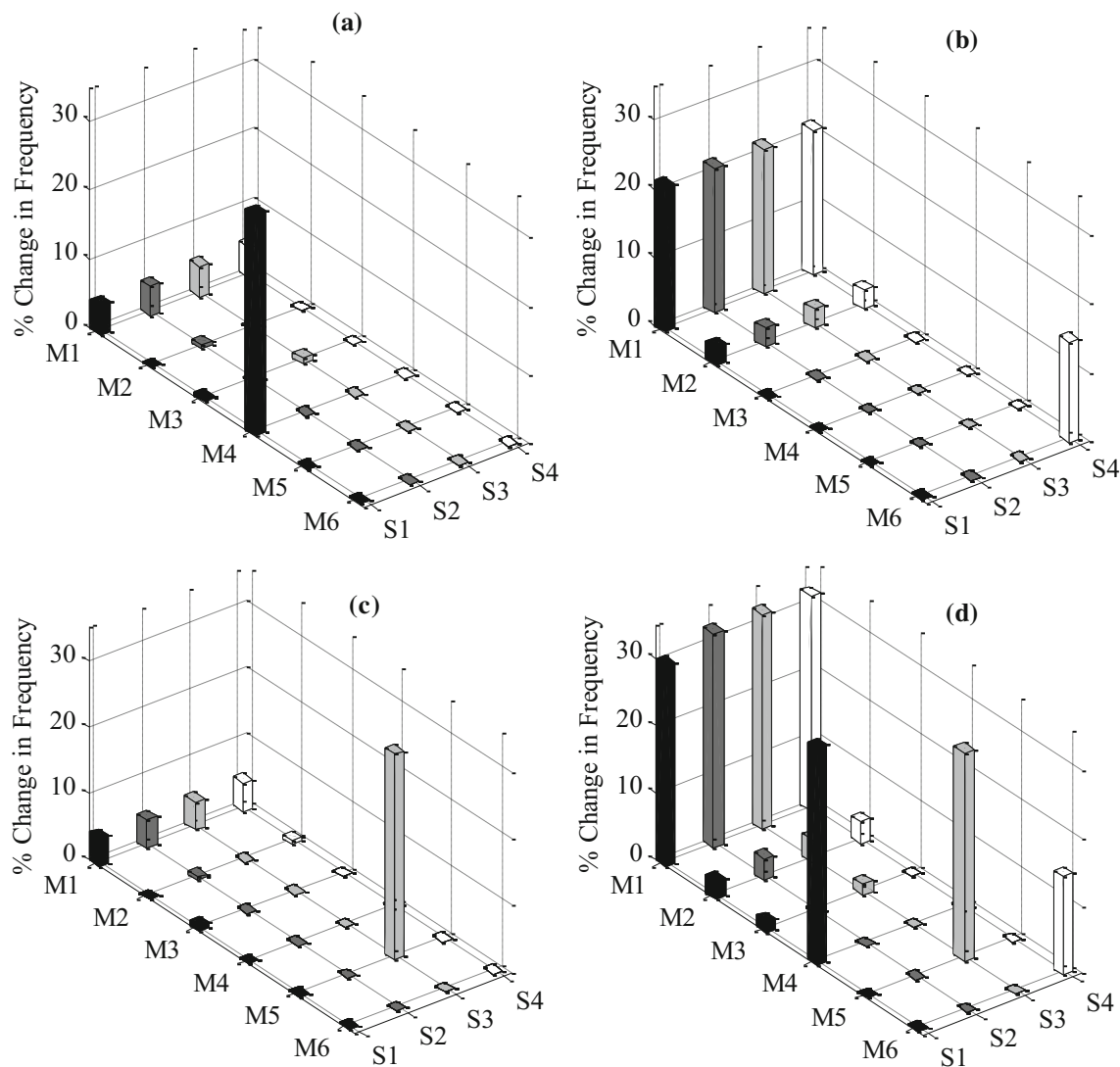
Fig. 13 Change in frequency of modes 1–6 detected at each sensor location S1 to S4. **a** Location A: LHS scour, **b** Location B: pier scour, **c** Location C: RHS scour, **d** Location D: all scour

From the analysis presented in Fig. 13, it is apparent that monitoring changes in particular modal frequencies can not only indicate the presence of scour affecting a structure, but can also potentially locate which element is affected by scour. For example if the data from sensor S1 are showing a small reduction in the frequency of mode M4 this would indicate potential scour of the LHS abutment. Alternatively, if sensor S1 is showing a small change in the frequency of M4, and sensor S4 is showing a large change in the frequency of M6 this would indicate that there is small scour of the LHS abutment and potentially large scour of the pier. This finding is predicated on the concept that modes local to a given element will be strongly affected by scour of that element, but otherwise relatively unaffected by scour elsewhere. This could be a particularly useful principle in multi-span bridges. In summary, it appears that

local vibration modes (e.g. M4–M6) are more sensitive to scour but it is acknowledged that they may be difficult to identify experimentally.

4.4 Effect of noise

Signals from actual sensors will contain measurement noise. To investigate if the presence of sensor noise will have a deleterious effect on the ability of the approach to reliably determine the bridge frequency, a brief analysis is conducted herein. The method for adding noise is based on the Signal-to-Noise Ratio (SNR) as presented in [40]. A discussion on adding noise to signals is available in [21]. Figure 14 shows the results of adding noise to the free vibration portion of acceleration signal generated at S2. Figure 14a contains a signal with an SNR of 20. Similarly,
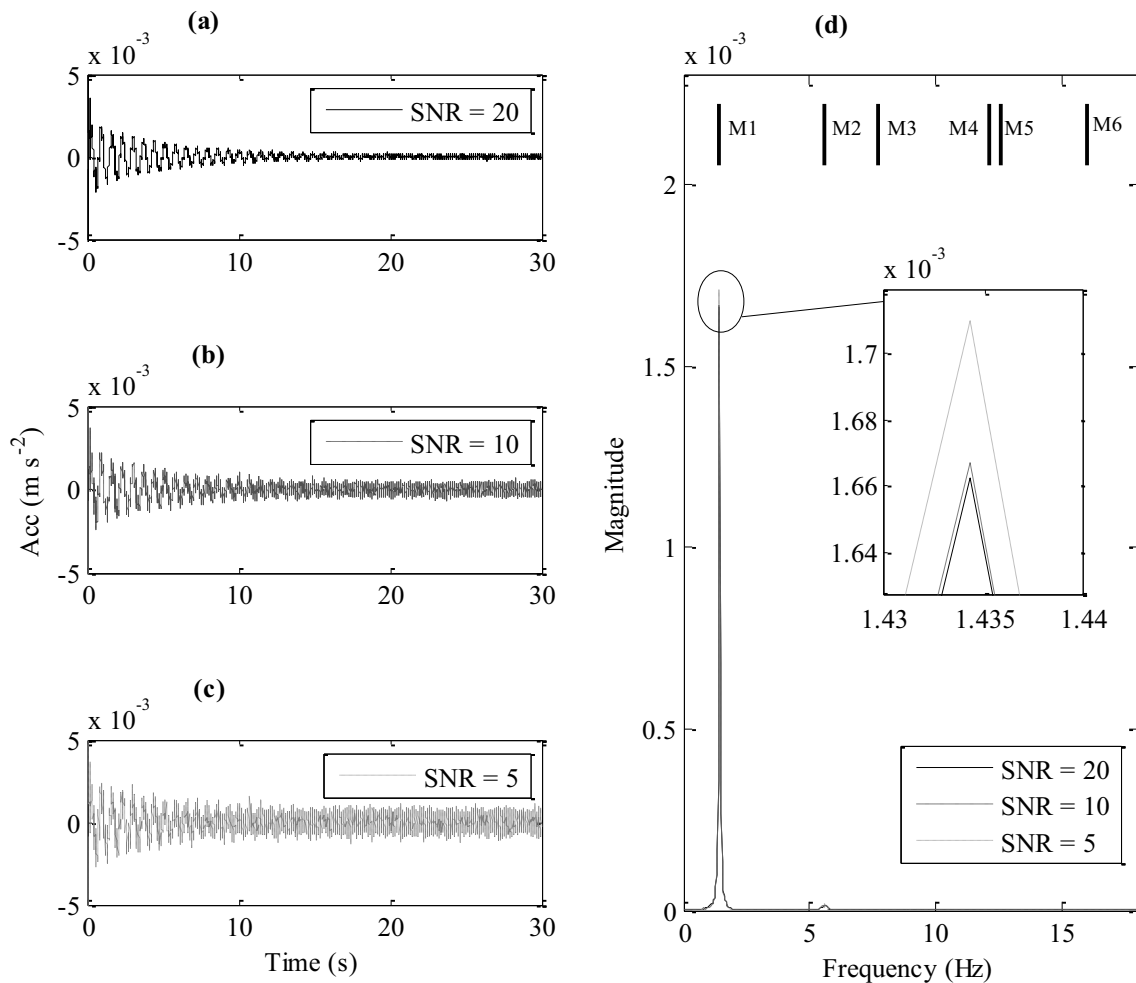
Fig. 14 Effect of added noise on frequency clarity—free vibration at sensor S2 after vehicle traverses at 30 km h^{-1}, **a** SNR = 20, **b** SNR = 10, **c** SNR = 5, **d** frequency of signals in (**a**) to (**c**) (*inset*) zoomed in at peak of frequency

Fig. 14b, c contains signals with SNRs of 10 and 5, respectively. Figure 14d shows the frequency content of the signals shown in (a) to (c). The frequency content is practically identical for each case with only minor differences in magnitude. It is, therefore, assumed that the approach will not be sensitive to noise.

5 Conclusions

The aim of this work was to investigate if scour location on an integral bridge can be determined from vibration measurements. To examine this, a bespoke vehicle–bridge–soil interaction model was developed and using an Eigenvalue analysis it was found that substructure elements (e.g. pier or abutments) have 'local' modes of vibration. The frequency associated with these modes is sensitive to scour adjacent to the element but is unaffected by scour elsewhere on the structure.

This local sensitivity to scour is potentially a very useful tool in identifying scour on a real bridge. However, on a real bridge frequencies cannot be determined using Eigen analyses, instead frequencies are determined by analysing dynamic response signals due to a passing vehicle. It is found that careful arrangement of the signal processing is necessary to accurately determine frequency. However, if care is taken with the signal processing it is found that the relevant 'local' frequencies could be identified and that by tracking the evolution of these frequencies it was possible not only to identify the occurrence of scour but more importantly to identify where scour had occurred.

In reality, it will be difficult to definitively identify scour as the causing mechanism for changes in frequency over other damage such as cracking or corrosion. However, if a frequency shift is due to scour, it is likely to be correlated to a flood event and potentially be quite large relative to the frequency shifts that occur from other types of damage such as corrosion, which tends to result in frequency

changes which are smaller and more gradual. Ultimately if frequency changes are identified on an element and scour is suspected, this could be used to trigger a manual inspection. Subsequently if the frequency change is found to have occurred due to some other form of damage, the end result is still useful to a bridge manager.

The results in this paper are promising; however, it is recommended that a field study be undertaken to validate the approach as part of future work. Experimental validation would be required before definitive conclusions on the efficacy of the approach can be given, since a real bridge may behave differently to a numerical approximation.

Moreover, the method is predicated on the ability to effectively identify local modes of a bridge. While this was successful in the numerical study undertaken, this may pose significant challenges in reality. The findings of this paper will nevertheless be useful to the ongoing development of the vibration-based scour monitoring field.

References

1. Melville BW, Coleman SE (2000) Bridge scour. Water Resources Publications, Highlands Ranch
2. Shirole AM, Holt RC (1991) Planning for a comprehensive bridge safety assurance program. Transp. Res. Rec. Transport Research Board, Washington, DC, pp 39–50
3. Forde MC, McCann DM, Clark MR et al (1999) Radar measurement of bridge scour. NDT&E Int 32:481–492
4. Wardhana K, Hadipriono FC (2003) Analysis of recent bridge failures in the United States. J Perform Constr Facil 17:144–151. doi:10.1061/(ASCE)0887-3828(2003)17:3(144)
5. Prendergast LJ, Gavin K (2014) A review of bridge scour monitoring techniques. J Rock Mech Geotech Eng 6:138–149
6. Briaud JL, Hurlebaus S, Chang K, Yao C, Sharma H, Yu O, Darby C, Hunt BE, Price GR (2011) Realtime monitoring of bridge scour using remote monitoring technology. Texas Department of Transportation, Austin
7. Hunt BE (2009) NCHRP synthesis 396: monitoring scour critical bridges—a synthesis of highway practice. Transportation Research Board, Washington, DC
8. Yu X (2009) Time domain reflectometry automatic bridge scour measurement system: principles and potentials. Struct Heal Monit 8:463–476. doi:10.1177/1475921709340965
9. Fisher M, Chowdhury MN, Khan A, Atamturktur S (2013) An evaluation of scour measurement devices. Flow Meas Instrum 33:55–67. doi:10.1016/j.flowmeasinst.2013.05.001
10. Anderson NL, Ismael AM, Thitimakorn T (2007) Ground-penetrating radar : a tool for monitoring bridge scour. Environ Eng Geosci XIII:1–10

11. Nassif H, Ertekin AO, Davis J (2002) Evaluation of Bridge Scour Monitoring Methods. New Jersey Department of Transportation, Trenton, NJ
12. De Falco F, Mele R (2002) The monitoring of bridges for scour by sonar and sedimetri. NDT&E Int 35:117–123
13. Zarafshan A, Iranmanesh A, Ansari F (2012) Vibration-based method and sensor for monitoring of bridge scour. J Bridg Eng 17:829–838. doi:10.1061/(ASCE)BE.1943-5592.0000362
14. Klinga JV, Alipour A (2015) Assessment of structural integrity of bridges under extreme scour conditions. Eng Struct 82:55–71. doi:10.1016/j.engstruct.2014.07.021
15. Ju SH (2013) Determination of scoured bridge natural frequencies with soil–structure interaction. Soil Dyn Earthq Eng 55:247–254. doi:10.1016/j.soildyn.2013.09.015
16. Prendergast LJ, Hester D, Gavin K (2016) Determining the presence of scour around bridge foundations using vehicle-induced vibrations. J Bridg Eng. doi:10.1061/(ASCE)BE.1943-5592.0000931
17. Chen C-C, Wu W-H, Shih F, Wang S-W (2014) Scour evaluation for foundation of a cable-stayed bridge based on ambient vibration measurements of superstructure. NDT&E Int 66:16–27. doi:10.1016/j.ndteint.2014.04.005
18. Prendergast LJ, Hester D, Gavin K, O'Sullivan JJ (2013) An investigation of the changes in the natural frequency of a pile affected by scour. J Sound Vib 332:6685–6702. doi:10.1016/j.jsv.2013.08.020i
19. Foti S, Sabia D (2011) Influence of foundation scour on the dynamic response of an existing bridge. J Bridg Eng 16:295–304. doi:10.1061/(ASCE)BE.1943-5592.0000146
20. Elsaid A, Seracino R (2014) Rapid assessment of foundation scour using the dynamic features of bridge superstructure. Constr Build Mater 50:42–49. doi:10.1016/j.conbuildmat.2013.08.079
21. Prendergast LJ, Hester D, Gavin K (2016) Development of a Vehicle-Bridge-Soil Dynamic Interaction Model for Scour Damage Modelling. Shock Vib 2016. Article ID 7871089. doi:10.1155/2016/7871089
22. Concast (2014) Concast Precast Group—Civil Engineering Solutions Brochure. http://www.concastprecast.co.uk/images/uploads/brochures/Concast_Civil.pdf. Accessed 1 May 2014
23. Kwon YW, Bang H (2000) The finite element method using MATLAB. CRC Press Inc, Boca Raton
24. Winkler E (1867) Theory of elasticity and strength. Dominicus, Prague **(in German)**
25. Dutta SC, Roy R (2002) A critical review on idealization and modeling for interaction among soil–foundation–structure system. Comput Struct 80:1579–1594. doi:10.1016/S0045-7949(02)00115-3
26. Prendergast LJ, Gavin K (2016) A comparison of initial stiffness formulations for small-strain soil–pile dynamic Winkler modelling. Soil Dyn Earthq Eng 81:27–41. doi:10.1016/j.soildyn.2015.11.006
27. Dukkipati RV (2009) Matlab for mechanical engineers. New Age Science, Kent
28. Tedesco JW, McDougal WG, Allen Ross C (1999) Structural dynamics: theory and applications. Addison Wesley Longman, California
29. Yang Y, Yau J, Wu Y (2004) Vehicle-bridge interaction dynamics. World Scientific, Singapore
30. API (2007) RP2A: Recommended practice for planning, designing and constructing offshore platforms—Working stress design. Washington, DC
31. API (ed) (2005) Recommended practice for planning, designing and constructing fixed offshore platforms—working stress design. API, Washington
32. Hester D, González A (2012) A wavelet-based damage detection algorithm based on bridge acceleration response to a vehicle.

Mech Syst Signal Process 28:145–166. doi:10.1016/j.ymssp.2011.06.007

33. González A, Hester D (2013) An investigation into the acceleration response of a damaged beam-type structure to a moving force. J Sound Vib 332:3201–3217. doi:10.1016/j.jsv.2013.01.024

34. Gonzalez A (2010) Vehicle-bridge dynamic interaction using finite element modelling. In: Moratal D (ed) Finite Element Analysis, Sciyo, pp 637–662. doi:10.5772/58224

35. Green F, Cebon D (1997) Dynamic interaction between heavy vehicles and highway bridges. Comput Struct 62:253–264

36. Yang F, Fonder G (1996) An iterative solution method for dynamic response of bridge–vehicles systems. Earthq Eng Struct Dyn 25:195–215

37. Cebon D (1999) Handbook of vehicle-road interaction. Swets & Zeitlinger, Netherlands

38. Farrar CR, Duffey TA, Cornwell PJ, Doebling SW (1999) Excitation methods for bridge structures. In: Proceeding of the 17th International Modal Analysis Conference (IMAC '99), Kissimmee, Fla, USA

39. Ülker-Kaustell M, Karoumi R (2011) Application of the continuous wavelet transform on the free vibrations of a steel–concrete composite railway bridge. Eng Struct 33:911–919. doi:10.1016/j.engstruct.2010.12.012

40. Lyons R (2011) Understanding digital signal processing, 3rd edn. Prentice Hall, Boston